JACS
JOURNAL OF THE AMERICAN CHEMICAL SOCIETY
Article
pubs.acs.org/JACS

Morphology of Liquid–Liquid Phase Separated Aerosols

Yuqing Qiu and Valeria Molinero*

Department of Chemistry, The University of Utah, 315 South 1400 East, Salt Lake City, Utah 84112-0850, United States

ABSTRACT: The morphology of liquid–liquid phase separated aerosols has a strong impact on their rate of gas and water uptake, and the type and rate of heterogeneous reactions in the atmosphere. However, it is extremely challenging to experimentally distinguish different morphologies (core–shell or partial wetting) of aerosols and to quantify the extent of wetting between the two phases. The aim of this work is to quantitatively predict the morphology of liquid–liquid aerosols from fundamental physical properties of the aerosol phases. We determine the equilibrium structure of liquid–liquid phase separated aerosols through free energy minimization and predict that the contact angle between the two liquids in the aerosol depends on the composition but not the amount of each phase. We demonstrate that for aerosols of diameter larger than ∼100 nm, the equilibrium contact angle can be accurately predicted from the surface tensions of each liquid with the vapor and between the two liquids through an expression that is identical to Young's equation. The internal structure of smaller, ultrafine aerosols depends also on the value of the line tension between the two liquids and the vapor. The thermodynamic model accurately predicts the experimental morphology, core–shell or partial wetting, of all aerosols for which surface tensions are provided in the literature, and provides contact angles that cannot be accurately determined with state of the art experimental methods. We find that the contact angle of model atmospheric aerosols is rarely higher than 30°. We validate the thermodynamic predictions through molecular simulations of nonane–water droplets, and use the simulation data to compute line tension values that are in good agreement with theory and the analysis from experimental data in water–nonane droplets. Our finding of a simple analytical equation to compute the contact angle of liquid–liquid droplets should have broad application for the prediction of the morphology of two-phase atmospheric aerosols and its impact in their chemistry.

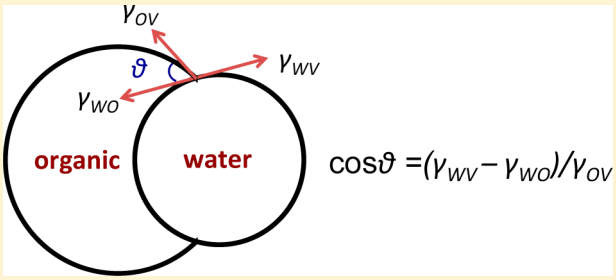

1. INTRODUCTION

Atmospheric aerosols have great impact on global climate by reflecting and absorbing solar radiation,[1,2] in their role as cloud condensation[3−10] and ice[11−15] nuclei, and as the locus of atmospheric chemical reactions.[16−20] The effect of aerosols on climate is influenced by both their chemical composition and morphology.[21−23] Two-phase aerosols can adopt different morphologies: core–shell (total wetting of one phase by the other) or partial wetting (asymmetric structures, with one phase partially engulfed by the other). The morphology of amorphous organic aerosols in the upper troposphere influences both the water uptake and heterogeneous ice nucleation on these particles.[14] The morphology also has an impact on N_2O_5 gas uptake by aqueous aerosols[24−31] and heterogeneous chemistry of HNO_3 with sea spray aerosols.[17,32] The morphology of aerosols is required to represent their physical properties, hygroscopicity and the kinetics of heterogeneous chemical reactions in climate models.[33] To create accurate representations for these climate models, it is important to determine to which extent each phase of the aerosol is exposed to the atmosphere.

There is a growing realization that aerosols particles that contain both organics and inorganics can undergo liquid–liquid phase separation when exposed to water vapor.[21,23,34−62] This phase separation alters the morphology of the aerosol particles. Because of their relevance to the atmospheric aerosols, most studies[36−38,46,50,51,53,55,63] focus on organics phase-separated from aqueous solutions containing inorganic salts. Inorganic salts promote liquid–liquid phase separation by salting-out.[64−66] However, a large number of organics separate from an aqueous phase even in the absence of salts.[42,67]

The structure of large (submicron and above) droplets has been studied using optical microscopy, optical tweezers, Raman spectroscopy, cryo-transmission electron microscopy (cryo-TEM), aerosol mass spectrometer (AMS) and scanning electron microscopy (SEM).[63] The contact angle between the two liquids, which measures the extent of wetting, cannot be derived from these experiments. Moreover, except for experiments with optical tweezers, the aerosols are usually deposited on a hydrophobic substrate. It has been shown that the hydrophobicity of the substrate may alter the equilibrium structure of the droplets.[68] Hence, the structure observed in these studies may not always correspond to the one the aerosols adopt in the atmosphere.

The elucidation of the internal structure of smaller, nanoscopic aerosols is even more challenging. However, recent advances have been made by the use of supersonic nozzles.[67,69,70] Wyslouzil and co-workers produced nonane–water nanodroplets through supersonic nozzle expansion, and

Received: May 29, 2015
Published: July 31, 2015

DOI: 10.1021/jacs.5b05579
J. Am. Chem. Soc. 2015, 137, 10642−10651

investigated their structure through small-angle X-ray scattering (SAXS) and Fourier transform infrared (FTIR) spectroscopy.[67] Modeling of the SAXS data was used to estimate the contact angles between water and nonane that represent the data gathered from the ensemble of binary nanodroplets.[70] Because of the inherent difficulty in determining the size of the particles and the contact angle between the two phases from the same data, the latter was estimated, with a very large uncertainty, to be between 40° and 120°.[67] Our goal in the present work is to predict the general morphology and values of the specific contact angles of two-phase liquid–liquid aerosols from thermodynamic properties of the liquids.

Spreading coefficients have been used to predict whether the equilibrium morphology of organic/aqueous droplets is core–shell, partial wetting, or nonwetting.[71] The spreading coefficients are defined by $S_2 = \gamma_{WV} - \gamma_{OV} - \gamma_{WO}$ and $S_3 = \gamma_{WO} - \gamma_{OV} - \gamma_{WV}$,[71] where W, O and V represent the aqueous, organic phase and vapor phases, respectively, and γ is the surface tension between the two phases designated by the subscript. When $S_2 > 0$ and $S_3 < 0$, the core–shell structure is adopted. When $S_2 < 0$ and $S_3 < 0$, the preferred structure involves partial wetting of the phase with highest liquid–vapor surface tension by the one with the lowest liquid–vapor surface tension. When $S_2 < 0$ and $S_3 > 0$, the formation of a liquid–liquid interface does not compensate for the loss of the two liquid–vapor surfaces and the two liquid droplets remain separate. Reid et al.[36,38,42] used values of spreading coefficients computed from bulk solutions to predict the morphology of aerosols containing both hydrophobic and hydrophilic components, and concluded that the partial wetting structure is predominant. Song et al.[46,55] used the same approach to predict the morphology of organic/ammonium sulfate/water systems, and found that the prevalent structure for liquid–liquid phase separated particles is core–shell, a conclusion also reached by Bertram et al.[41] and Ciobanu et al.[37] Although spreading coefficient can be used to distinguish partial wetting from core–shell morphologies, they cannot be used to quantify the extent of partial wetting, the contact angle between the two phases in the aerosol.

Kwamena et al.[38] used an iterative approach to predict the morphology of liquid–liquid phase-separated particles by minimizing the surface free energy with respect to the degree of insertion between the two liquids and the curvature of the liquid–liquid interface. This method can converge to the optimum structure numerically, but it does not provide an analytical equation to determine the morphology. Torza and Mason proposed that the equilibrium morphology of two-phase droplets could be analytically computed assuming that the interfacial forces, with magnitude given by the surface tensions and with direction tangential to the liquid–liquid and liquid–vapor interfaces at the point of three-phase contact, add up to zero.[71] Buajarern et al.[36] examined the morphology of two-phase droplets using that methodology and concluded that the equilibrium configuration of two-phase liquid droplets depends on the three surface tensions and the volume ratio between the two phases. In this work we reconsider this issue through thermodynamic modeling and molecular simulations of liquid–liquid separated droplets.

Several physical factors could affect the morphology of the liquid–liquid phase separated aerosols: the amount of each phase, temperature, and properties of the liquid phases such as surface tensions, line tension, and the dependence of the Laplace pressure on the degree of wetting. In this work, we develop a thermodynamic model to investigate which of these factors are important in determining the equilibrium morphology of aerosols, and quantify the extent of wetting in the two phase liquid–liquid aerosols of arbitrary composition and size. We derive simple relations for the contact angle between the two phases in the droplet as a function of the surface tensions and validate the thermodynamic predictions with molecular simulations of two-phase liquid aerosols.

2. THERMODYNAMIC MODELING OF THE MORPHOLOGY OF LIQUID–LIQUID AEROSOLS

2.1. Free Energy of Two-Phase Aerosols Is a Function of Their Internal Structure. We first develop a thermodynamic model that allows us to minimize the free energy of two-phase liquid droplets with respect to the shape of the domains of its two phases. Here we call the phases water (W) and organic (O), but they can be any pair of liquid phases sufficiently large to have a homogeneous interior (e.g., for water, at least 100 molecules[72]). The difference in free energy between the equilibrium two-phase droplets and the corresponding amount of bulk W and O liquid is given by

$$\Delta G = \gamma_{WV}A_{WV} + \gamma_{OV}A_{OV} + \gamma_{WO}A_{WO} + \tau 2\pi R_b + \int_{p_0}^{p_O} V_O \, dp + \int_{p_0}^{p_W} V_W \, dp \quad (1)$$

where γ_{WV}, γ_{OV} and γ_{WO} are, respectively, the W–vapor, O–vapor, and W–O surface tensions; A_{WV}, A_{OV} and A_{WO} represent the areas of the W–vapor, O–vapor and W–O interfaces; $2\pi R_b$ is the length of the three-phase contact line between W, O and vapor, and τ is the corresponding line tension. τ can be either positive or negative and typically has a magnitude of the order of 10^{-12} N.[73−76] p_W and p_O are the interior pressures of the W and O droplets, which are the sum of exterior pressure and the Laplace pressure drop across the interfaces of the W and O liquids. The internal pressures depend on the curvature of these phases. p_0 is the reference pressure at which the free energies of the bulk W and O phases are determined. In what follows, the liquid with the higher liquid–vapor surface tension is called W.

To evaluate the free energy, we need to determine how the areas and line of contact in eq 1 change with the degree of wetting. This depends on the curvature of the WO interface. This interface can be flat only when the Laplace pressures on the two phases are identical, i.e., when they have the same ratio of the surface tension of the liquid–vapor interface to the radius of the phase, $\gamma_{OV}/R_O = \gamma_{WV}/R_W$. In all other cases, the aerosol will have a curved WO interface. In this work, we consider that W forms a sphere that is partially wetted by O. This has been called the idealized "Russian doll"[67,77] (RD) or lens on a sphere model, and is shown in Figure 1. The actual WO interface could have a curvature intermediate between the spherical cap of the idealized RD and a flat surface, determined by the competition between elastic and capillary forces in the droplet.[78] As all models with intermediate curvature of the WO surface have almost the same liquid–vapor contour, in what follows we first find the contact angle between W and O that minimizes the free energy of the RD model, and then discuss how the contact angle would change if the WO surface were allowed to deform.

The free energy with respect to the separate bulk phases can be derived from eq 1 and the geometry of the model. Using r_W and r_O for the radii of the spherical section of W and O, and h_W

DOI: 10.1021/jacs.5b05579
J. Am. Chem. Soc. 2015, 137, 10642−10651

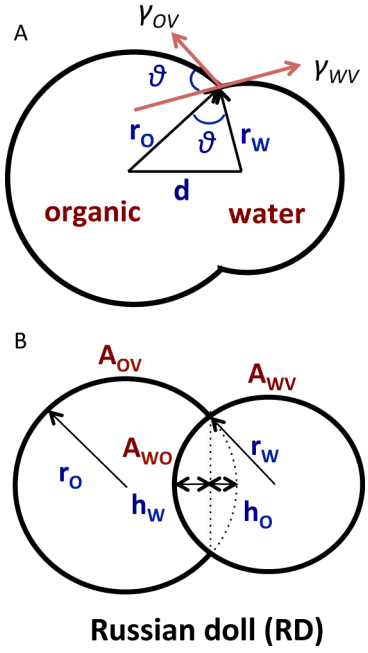

Figure 1. Internal structure of two-phase droplets with partial wetting morphology. (A) Liquid–vapor contour of two-phase droplets with contact angle θ between the W and O phases of radii r_W and r_O, respectively, and distance d between the centers of the two spherical caps that define each liquid phase. The angle formed by the tangents to the WV and WO surfaces is $180° - \theta$. Core–shell droplets have contact angle 0°, nonwetting droplets a contact angle of 180°, and partially wetting droplets a value in between. (B) Internal structure of the idealized Russian doll (RD) model, where h_W and h_O are the height of the overlapped spherical caps, and A_{WV}, A_{OV} and A_{WO} represent the areas of the W–vapor, O–vapor and W–O interfaces, respectively.

and h_O for the height of the overlapped spherical caps (Figure 1), we write ΔG of the RD model:

$$\Delta G_{RD} = \gamma_{WV}(4\pi r_W^2 - 2\pi r_W h_W) + \gamma_{OV}(4\pi r_O^2 - 2\pi r_O h_O) + 2\gamma_{WO}\pi r_W h_W + \tau 2\pi R_b + \int_{p_0}^{p_O} V_O \, dp + \int_{p_0}^{p_W} V_W \, dp \quad (2)$$

The contact angle θ between two phases (Figure 1) is the angle formed by r_W and r_O with the segment d that measures the distance between the centers of each phase:

$$\theta = \cos^{-1}((r_W^2 + r_O^2 - (r_W + r_O - h_W - h_O)^2)/(2r_W r_O)) \quad (3)$$

To find the optimum structure of the two-phase droplets, we minimize the free energy of the model with respect to θ. There are three types of contributions to the free energy in eq 1 arising from the surface tensions, the line tension, and the Laplace pressures. These contributions have different scaling with the radii of the phases, r. The γA terms are proportional to r^2. The line tension is roughly proportional to r, and the Laplace pressure term is proportional to r^{-1}. For all droplets, we assume that the volume of each liquid and the Laplace pressures are independent of the degree of insertion d between the two phases. The Laplace terms then are constants and can be neglected. In section 3 we validate this assumption with molecular simulations of two-phase droplets.

2.2. Contact Angle in Large Liquid–Liquid Aerosols.

Whenever a WO interface is formed, it costs a W–vapor interface and an O–vapor interface of the same area. We first derive the boundary of partial wetting with respect to surface tension ratios γ_{OV}/γ_{WV} and γ_{WO}/γ_{WV} in the limit of large droplets, for which the line tension contribution can be neglected (recall that we call the phase with higher surface tension W). When $\gamma_{WO} > \gamma_{WV} + \gamma_{OV}$, the total free energy increases with the appearance of WO interface and the two phases will remain as separate droplets (nonwetting case). When $\gamma_{WO} < \gamma_{WV} - \gamma_{OV}$, the formation of WO interface always decreases the total free energy, and W will be fully covered by O. Partial wetting droplets are formed between these two boundaries, when $\gamma_{WV} - \gamma_{OV} < \gamma_{WO} < \gamma_{WV} + \gamma_{OV}$. The boundaries of nonwetting, partial wetting and total wetting for large droplets depend only on the surface tension ratios γ_{OV}/γ_{WV} and γ_{WO}/γ_{WV} and are shown in Figure 2. The boundaries obtained by free energy minimization are the same as derived by Torza and Mason[71] using spreading coefficients.

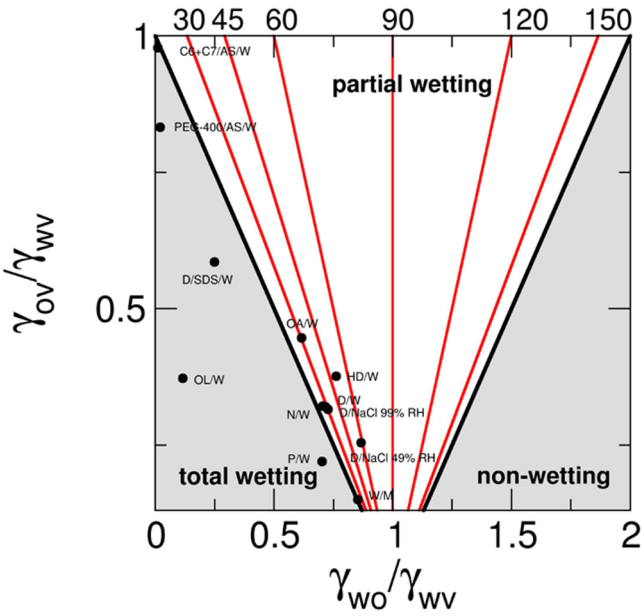

Figure 2. Morphology map for liquid–liquid phase separated Russian doll model droplets as a function of the ratio of surface tensions in the large droplet limit. The circles represent data for model aerosols reported in the literature (see Table 1). Gray regions correspond to total wetting (θ = 0°) or nonwetting (θ = 180°). The white area corresponds to the partial-wetting region. Red lines correspond to constant θ (values shown at the top of each line) computed with eq 4.

The contact angle θ between the two phases in the droplet quantifies the extent of wetting: θ = 180° corresponds to nonwetting, and θ = 0° to core–shell. These are the only two limits that can be derived from the comparison of spreading coefficients. The thermodynamic model of this work, however, can predict the equilibrium contact angle of aerosols as a function of the surface tensions and, for nanodroplets, also the line tension. We compute the contact angle in the limit of large droplets by minimization of the free energy of the aerosols with respect to θ considering only the first three terms in the right hand side of eq 2.

Our analysis indicates that θ depends on the three surface tensions but is independent of the volume of each phase. The

DOI: 10.1021/jacs.5b05579
J. Am. Chem. Soc. 2015, 137, 10642–10651

Table 1. Morphology and Contact Angle of Aerosols Predicted from Surface Tensions

label	composition	γ_{OV} (mJ/m^2)	γ_{WO} (mJ/m^2)	γ_{WV} (mJ/m^2)	morphology[h]	θ_Y[i] (deg)	θ_N[j] (deg)
P/W	pentane/water	15.9[a]	50.9[a]	72.4[b]	CS	0	0
N/W	nonane/water	22.7[a]	52.4[a]	72.4[b]	PW	28	24
HD/W	hexadecane/water	27.2[a]	55.2[a]	72.4[b]	PW	51	42
M/W[c]	mercury/water	72.75[c]	415[d]	486.5[d]	PW	11	10
C6+C7/AS/W[e]	dicarboxylic acids with 6 and 7 carbons/ammonium sulfate/water	40.7	0.5	41.6	CS	0	0
PEG-400/AS/W[f]	polyetheylene glycol400/ammonium sulfate/water	42.6	1.1	51.2	CS	0	0
OL/W[g]	octanol/water	27.1	8.5	72.8	CS	0	0
OA/W[g]	oleic acid/water	32.5	44.9	72.8	PW	31	23
D/W[g]	decane/water	23.4	51.3	72.8	PW	23	19
D/SDS/W[g]	decane/sodium dodecyl sulfate/water	23.4	10.0	40.0	CS	0	0
D/NaCl/99% RH[g]	decane/NaCl at 99% RH	23.4	52.4	73.2	PW	27	23
D/NaCl/49% RH[g]	decane/NaCl at 49% RH	23.4	79.7	91.9	PW	59	52

[a]ref 87 T = 295 K. [b]ref 88 T = 295 K. [c]ref 88 T = 293 K. [d]ref 89 T = 293 K. [e]ref 46 T = 293 K. [f]ref 46 T = 298 K. [g]ref 38. [h]CS indicates core−shell and PW partial wetting. [i]Contact angle θ_Y computed from Young relation (eq 4), [j]Contact angle θ_N computed from Neumann's relation (eq 5).

contact angle that minimizes the free energy of large idealized RD droplets is

$$\cos\theta = (\gamma_{WV} - \gamma_{WO})/\gamma_{OV} \quad (4)$$

which is identical to Young equation[79] for the contact angle of a liquid droplet on a solid substrate, $\cos\theta = (\gamma_{sv} - \gamma_{sl})/\gamma_{lv}$, if we consider the liquid with the highest liquid−vapor surface tension, W, plays the role of the nondeformable solid phase. The same mathematical solution was originally derived by Fletcher,[80] and later extended by other authors,[81−83] for heterogeneous nucleation on convex spherical substrates. We refer to these studies for mathematical steps in the derivation of eq 4. The lines of constant θ in the partial wetting region of the morphology map for large droplets form a fan-shaped distribution (Figure 2).

Young equation is the solution for the elastocapillary equilibrium in large droplets when one phase (W of the RD model) does not deform under the action of capillary forces, while the other phase (O of the RD model) can be deformed without eliciting elastic stress. If the two phases can deform without elastic resistance, the condition of equilibrium in large droplets requires the balance of the three surface tensions at the contact line.[84,85] To achieve this balance, the WO and WV interfaces adopt different curvatures. Neumann's triangle describes the relation of the angles between the phases in terms of the surface tensions when the contribution from elastic forces and line tension are negligible.[78,84] The contact angle between W and O that results from the geometry of Neumann's triangle is given by

$$\cos\theta = (\gamma_{WV}^{\ 2} + \gamma_{OV}^{\ 2} - \gamma_{WO}^{\ 2})/(2 \times \gamma_{WV} \times \gamma_{OV}) \quad (5)$$

Liquids have low shear moduli,[86] hence eq 5 may provide a more accurate description of the contact angle in liquid−liquid droplets than eq 4. Nevertheless, as we illustrate in next paragraph, the contact angles predicted by these two limiting elastocapillary scenarios are very close.

Table 1 summarizes the morphology and contact angles we predict for liquid−liquid phase separated aerosols using surface tensions reported in the literature and eqs 4 and 5. For all aerosols, the morphologies predicted by the thermodynamic model, core−shell (CS) or partial wetting (PW) are in agreement with the experiments. θ_Y predicted from Young's relation is always slightly larger than θ_N predicted from Neumann's construction. However, if the uncertainty in the surface tensions were 1 mJ/m^2, then the difference between the predicted θ_Y and θ_N would be smaller than their error bars. Recent advances in the determination of surface tensions for micron and submicron-sized aerosols using AFM,[90] would make possible to predict the morphology of complex atmospheric particles without the need of producing the same mixtures in bulk quantities.

Most two-phase liquid aerosols are located in the narrow area along the total wetting boundary with contact angle smaller than 30°. Only two model aerosols, hexadecane/water and decane/NaCl at 49% RH, have θ between 30° and 60°. These aerosols either have a very hydrophobic O phase or a high salt concentration. Based on the hydrophobicity of these phases, we expect the contact angle θ to be smaller than 60° in most, if not all, liquid−liquid phase separated atmospheric aerosols.

Surfactants, such as myristic acid, palmitic acid, stearic acid, phospholipids and glycolipids, naturally occur in atmospheric aerosols.[91−95] The presence of surfactants in the aqueous phase decreases γ_{WO} faster than γ_{WV}, turning the morphology of aerosols from partial wetting to core−shell. An example of this transformation is seen in Figure 2 and Table 1: decane/water droplets have a core of water partially covered with the alkane, while decane/SDS/water droplets are core−shell.[38] In general, the presence of salts increases γ_{WO} faster than γ_{WV}. Hence, the surface tension ratios move toward the bottom right of the morphology map (Figure 2), approaching the nonwetting region. For example, when decane/NaCl(aq) droplets are equilibrated at low relative humidity, the extent of partial wetting decreases.[38] In conclusion, analysis of extensive literature data presented in Table 1 shows that two-phase aerosols of atmospherically relevant compositions are located near the boundary between partial wetting and total wetting in the morphology map. Our analysis reconciles the apparently inconsistent claims of researchers that found partial wetting or core−shell structures when investigating the structure of model aerosols[38,46] and provides simple analytical relations to compute the contact angle between the liquid phases in the aerosols from knowledge of the surface tensions of these liquids.

2.3. Line Tension Corrections to the Contact Angle of Two-Phase Nanodroplets. In the previous discussion, we addressed the structures in the limit of large droplets, for which the contribution of the line tension between W and O phases,

DOI: 10.1021/jacs.5b05579
J. Am. Chem. Soc. 2015, 137, 10642−10651

$\tau 2\pi R_b$, is negligible with respect to the surface terms. We now consider the contribution of the line tension τ to the free energy of nanodroplets. τ can be positive or negative. A positive τ increases the repulsion between the two phases, and the total free energy decreases by approaching either the core−shell (θ = 0°) or nonwetting (θ = 180°) morphologies. As a result, a positive τ narrows the domain of partial wetting. On the other hand, a negative τ increases the attraction between the two phases resulting in widening of the domain of partial wetting. Figure 3 shows the morphology map for nanodroplets of 50

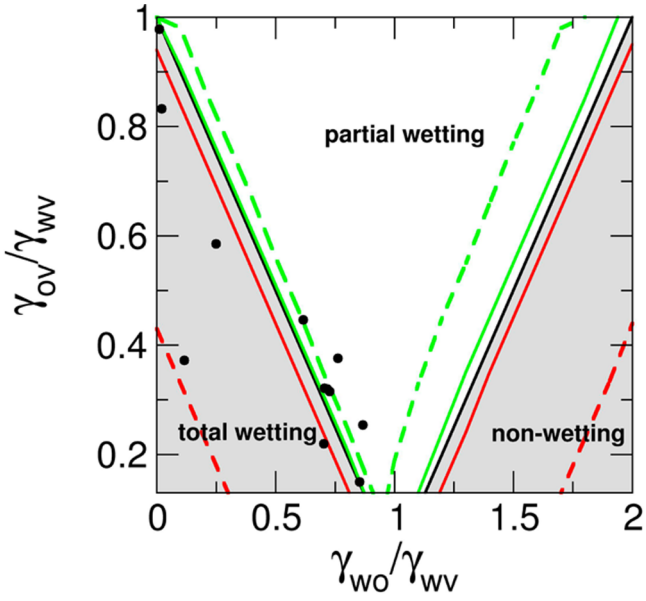

Figure 3. Morphology map for different sizes of Russian doll model droplets. Boundaries of the partial wetting region for droplets with radii of each phase 5 nm (dashed red and dashed green lines), 50 nm (solid red and solid green lines), and in the large-droplet limit (solid black lines). Green lines correspond to line tension τ = 20 pN, and red lines to τ = −20 pN. Dots are the same as in Figure 2.

and 5 nm radii. For both droplet sizes, positive τ narrows the partial wetting region and negative τ expands it. The effect, however, is dramatic only for the 5 nm droplets: surface tensions that would lead to total wetting in the large droplet limit result in partial wetting if τ = −20 pN. Positive τ = 20 pN affects those 5 nm droplets near the boundary and convert them to core−shell. For the 50 nm droplets, on the other hand, changes in boundaries with respect to τ are tiny. We conclude that the internal structures of aerosols with radii as small as 50 nm are already like those of their large counterparts.

Young equation is an exact solution for the contact angle of the idealized RD model in the limit of large droplets, when the line tension term can be neglected. To further quantify the extent of partial wetting for nanodroplets, we add the line tension to the free energy of the Russian doll model eq 2 and investigate how θ depends on τ. The relation that results is an extension of Young's equation:

$$\gamma_{WO} - \gamma_{WV} + \gamma_{OV} \times \cos\theta + \frac{R_W - R_O \times \cos\theta}{R_W \times R_O \times \sin\theta}\tau = 0 \quad (6)$$

which has been previously derived in refs[81,82] for the mathematically equivalent problem of nucleation of a liquid on a curved surface.

Figure 4 shows $\theta(\tau)$ obtained by numerical solution of eq 6 for several sizes of water−nonane droplets at 308 K. The

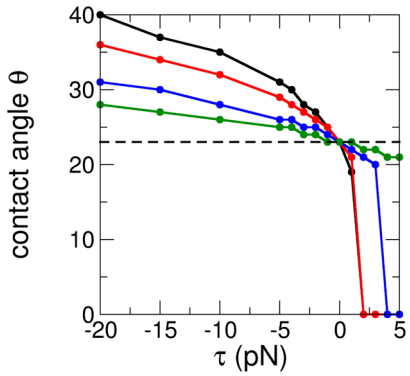

Figure 4. Sensitivity of the contact angle θ of water−nonane nanodroplets to the line tension. In the case considered in this figure, the contact angle for large droplets is 23° (dashed line). Each color represents θ of droplets with different radii of nonane and water domains: black corresponds to r_n = 7 nm and r_w = 3 nm, red to r_n = 10 nm and r_w = 5 nm, blue to r_n = 22 nm and r_w = 10 nm, and green to r_n = 48 nm and r_w = 23 nm. As expected, θ of the smaller nanodroplets is the most sensitive to the line tension.

contact angle of nanodroplets can sharply collapse to 0°, total wetting, with positive τ. Phase compositions that result in partial wetting morphology for large droplets, may produce core−shell nanodroplets under the impact of positive τ. Similarly, if θ for a large droplet were close to 180°, a case we consider highly improbable in atmospheric aerosols, repulsion between the two phases induced by positive τ would force the nanodroplet to turn into two separated droplets, i.e., an externally mixed aerosol.

Nonane−water nanodroplets have been produced and studied in supersonic nozzles starting with a stagnation temperature of 308 K, and cooled to ∼230 K during the expansion.[67,70,96] The contact angles predicted from the experimental surface tensions[88,97,98] at 308 K are 23° and 19.4° in the Young and Neumann regimes, respectively, and quite insensitive to temperature (e.g., with the surface tension values at 283 K, Young equation predicts θ = 26°, and with surface tensions extrapolated to 233 K, it predicts θ = 29°). Modeling of the SAXS spectra of nonane−water droplets assuming a Russian doll model with nonane and water phases of radii 11 and 5 nm, respectively, indicates that θ could be between 40° and 120°.[67] It should be noticed that the SAXS signal depends both on the contact angle and the radii of the droplets,[70] and the aerosols generated by the nozzle are polydisperse.[67] The difficulty of deriving the contact angle and size of two-phase droplets while accounting for the polydispersity of the droplets accounts for the uncertainty in θ. Theoretical considerations indicate that τ between *n*-alkanes and water must be smaller than 5 pN.[74] We find that a value of line tension τ close to −30 pN at 233 K (−28 pN at 308 K) is needed to produce θ = 40 ± 1° for r_n = 11 nm and r_w = 5 nm nonane−water droplets, assuming (as in the literature[67,70]) that they have an idealized Russian doll internal structure. In next section, we use simulations to validate the assumptions of the thermodynamic model and to compute the line tension between nonane and water from molecular simulations with the OPLS and mW models, respectively. We find it to be −21 pN at 295 K, in good agreement with the value needed to

DOI: 10.1021/jacs.5b05579
J. Am. Chem. Soc. 2015, 137, 10642−10651

reconcile the contact angle predicted from the experimental surface tensions and the one deduced from the modeling of SAXS data.

3. MOLECULAR SIMULATIONS VALIDATE THERMODYNAMIC PREDICTIONS

To verify the accuracy of the predictions of the thermodynamic model discussed in Section 2, we perform simulations of two-phase nonane–water droplets, as their internal structure has been the focus of recent experimental[67] and simulation[70] studies. We first verify that they adopt the partial wetting Russian Doll morphology. We then compute the contact angles of the nanodroplets as a function of the size of each phase, validate our assumption that even for nanodroplets the impact of Laplace pressure terms on the contact angle is negligible, and determine the line of tension for the molecular model.

3.1. Simulation Methods. Molecular dynamics (MD) simulations are performed with LAMMPS.[99] The equations of motion are integrated with the velocity Verlet algorithm using a time step of 5 fs and periodic boundary conditions. Nonane is modeled with the united-atom (UA) OPLS alkane force field, which represents each $-CH_3$ and $-CH_2$ groups by single particles that interact through Lennard–Jones potentials.[100,101] Water is modeled with the monatomic water model mW, which represents each water molecule as a single particle that interacts through short-ranged two- and three-body interactions that mimic tetrahedral hydrogen-bonding interactions.[102] The mW model has been extensively validated for the simulation of liquid water, droplets, hydrophobic interactions, interfacial properties, and phase transitions.[72,102−124] The liquid–vapor surface tension of mW water is 66 mN/m at 295 K,[110] comparable to the 68.8 mN/m reported for the best fully atomistic nonpolarizable model of water, TIP4*P*/2005,[119] and within 10% of the experimental value (Table 2).

Table 2. Surface Tensions of Nonane-Vapor γ_{nv}, Nonane–Water γ_{nw}, and Water–Vapor Surface Tension γ_{wv} in the Molecular Simulations and in Experiments

surface tension[a]	simulations	experiment
γ_{nv} (mJ/m^2)	23 ± 0.9	22.7[b]
γ_{nw} (mJ/m^2)	51 ± 1.2	52.4[b]
γ_{wv} (mJ/m^2)	66 ± 0.7[c]	71.99[d]

[a] γ_{nv} and γ_{nw} at 295 K and γ_{wv} at 298 K. [b] ref 87. [c] ref 119. [d] ref 88.

The OPLS nonane–vapor surface tension, has not been previously reported in the literature. We compute it from the pressure tensor components normal (p_n) and tangential (p_t) to the interface,[125] $\gamma = (L_z/2)[\langle p_n\rangle - \langle p_t\rangle]$, averaged over 50 ns *NVT* simulations with slabs containing 114 nonane molecules. We find that the surface tension of OPLS nonane (Table 2) is within 1.3% of the experimental value. We parametrize the nonane–water interactions by matching the nonane–water surface tension γ_{nw} to the experimental value at 295 K (Table 2). γ_{nw} is determined from 50 ns *NVT* simulations with slabs containing 114 nonanes in contact with 1024 water molecules. In the parametrization, methyl and methylene groups are considered to interact identically with water through a Lennard-Jones potential. The size σ_{wm} = 0.35 nm of water–methylene interaction is the average of SPC/E[126] water–water distance σ_{ww} and OPLS alkane methylene–methylene distance σ_{mm}.[100] We tune water–methylene interaction ε_{wm} for nonane–water interface to reproduce γ_{nw}. The strength between water-methylene that reproduces the experimental nonane-water surface tension (Table 2) is ε_{wm}= 0.17 kcal/mol.

3.2. Structures of Droplets in Simulation Agree with Thermodynamic Predictions. We perform simulations of two-phase liquid droplets of OPLS nonane and mW water with the aim of verifying whether the morphologies of these ultrafine aerosols are consistent with the predictions of a thermodynamic model derived under the assumption that (i) the change in Laplace pressure with respect to contact angle is negligible and (ii) the contribution from the line tension is only important in small nanodroplets. The contact angle derived from the surface tensions of the OPLS nonane and mW water models at 295 K using Young's equation is 49 ± 9°. This is the solution of the free energy minimization of the RD model when both the line tension and the Laplace pressure contributions are neglected. The error bar accounts for the uncertainty in the surface tensions (Table 2). The contact angle predicted from the surface tensions of the molecular models is different from the θ = 23° predicted from the experimental surface tension at the same temperature, although only the surface tension of water in the simulations deviates, by less than 10%, from the experimental value. This indicates that accurate surface tensions are essential to predict the exact contact angle of atmospheric aerosols. Our goal here is not to reproduce the experimental contact angles, but to validate the thermodynamic model by comparing the contact angle predicted from the surface tensions of the OPLS nonane and mW water with the one determined from a structural analysis of binary droplets simulated with the same molecular models.

The simulated droplets contain between 2000 and 32 000 molecules. The droplets are first equilibrated for 50 ns in canonical simulations at 295 K, starting from separated slabs of water and nonane. The morphology is computed from the density distribution averaged over 1000 configurations recorded over 2.5 ns after equilibration. The locus of the interfaces is defined by the surface at which the density drops to half of the bulk density. The edges of both liquid phases are fit to spherical caps, from which the contact angle θ is computed through eq 3.

All water–nonane droplets are well represented by the Russian doll morphology (Figure 5), in agreement with previous simulations of PYS nonane-SPC/E water droplets.[70,127] The largest droplets here have radii of 10 nm, so all these droplets are small enough that we must consider the impact of the line tension on θ. Nevertheless, the contact angles of all the droplets are within 7° of θ = 49° given by the thermodynamic prediction of the RD model in the large droplet limit (Table 3); i.e., the effect of the line tension is within the uncertainty that results from propagating the error of the surface tensions in Table 2. As the line tension τ for this system is not available, we find the value of τ that best reproduces the simulation results by first computing the equilibrium contact angle as a function of τ for each droplet and then finding the range of τ values that reproduces θ within ±1° from the simulation result. The optimum τ is −21 pN (Table 3). τ derived for the molecular model is consistent with the τ estimated in section 2 from the contact angle derived from SAXS data[67] and also with the range calculated for water-alkane interfaces in the theory of Cahn.[74] As the contribution of the line tension scales with the radius R of the phase and those of the Laplace pressure with R^{-1}, the ability to recover the contact angle in the simulations with only the surface tension and line tension terms validate our assumption that the change in

DOI: 10.1021/jacs.5b05579
J. Am. Chem. Soc. 2015, 137, 10642−10651

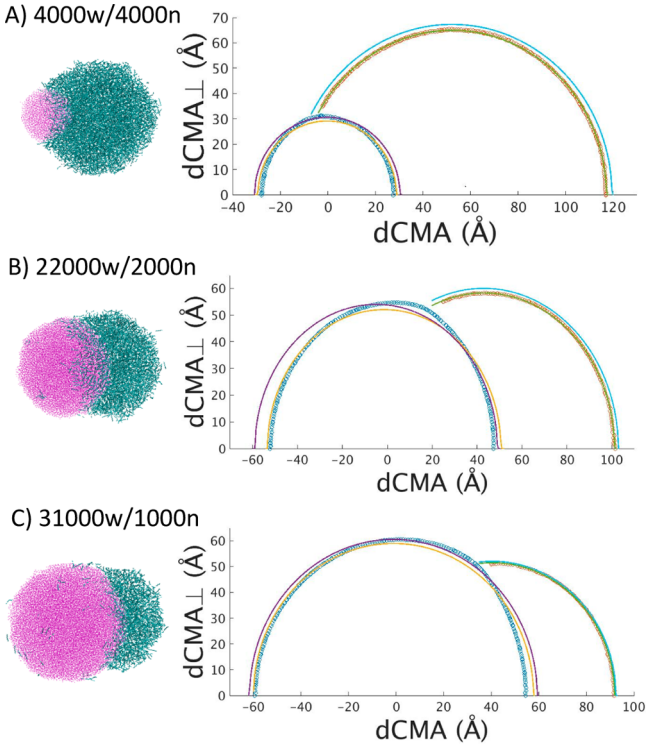

Figure 5. Morphology of nonane-water aerosols from molecular simulations with the OPLS and mW water models. Droplets in A, B and C panels have almost identical total volume but different water:nonane ratio. Left: snapshots of the droplets with water shown with pink points and nonane with cyan sticks. Right: the corresponding density profiles for water (blue) and nonane (red) as a function of the distances to the center of mass (CM) in the axes parallel and perpendicular to line that joins the center of mass of the two liquids. Yellow and green lines show the fits of these density profiles to spherical caps, and purple and blue lines the profiles predicted for perfect Russian doll morphology (water in purple and nonane in blue) with the contact angle predicted by eq 4, which does not account for the line tension correction.

Table 3. Contact Angle θ in Nonane-Water Droplets at 295 K from the Simulations and from Thermodynamic Prediction with $\tau = -21$ pN[a]

N_{nonane}/N_{water}	θ from RD fit (deg)	predicted θ from RD thermo model with $\tau = -21$ pN (deg)
1000/1000	56 ± 2	55 ± 6
4000/4000	53 ± 1	53 ± 6
16000/16000	52 ± 1	52 ± 6
2000/22000	47 ± 1	46 ± 7
1000/31000	44 ± 1	43 ± 10

[a]Large-droplet limit $\theta = 49°$ eq 4.

Laplace pressure with the contact angle has a negligible contribution to the equilibrium morphology of aerosols, even in the case of nanoparticles for which the Laplace pressure itself is not negligible.

The small deviations from a perfect spherical geometry in the density profiles of Figure 5 suggest that water and nonane are deformable under the effect of the capillary forces. We now assume that we can disregard the elastic forces and rely on Neumann's construction to compute the line tension. The generalization of Neumann's triangle to include line tension is a quadrilateral construction in which the line tension adds a new component to the interfacial forces in the direction of the radius of the contact line.[128] We calculate the direction of the surface tension forces as the tangent to the simulation density profiles (Figure 5) at the line of three-phase contact. Due to the small size of the droplets, the surfaces curve at short distances from the three-phase contact line. We use 0.05 nm segments to estimate the tangents, and Neumann's quadrilateral construction of ref[128] to estiomate the line tension for each droplet. This results in a highly dispersed set of positive and negative values for τ. As there is a single value of τ for each combination of phases, we conclude that the tangents extracted from the simulation profiles of these small droplets are not sufficiently accurate to estimate τ in the Neumann limit.

To further validate the thermodynamic predictions, we compute the contact angle of droplets with 4000 waters and 4000 nonanes in which we modify the water–nonane surface tension γ_{nw} by tuning the water-methylene attraction ε_{wm} (Table 4). As expected, the contact angle becomes smaller with decreasing free energy cost of the liquid–liquid interface (Figure 6). When $\gamma_{nw} < \gamma_{wv} - \gamma_{nv}$, total wetting is observed in the simulations, as predicted by the thermodynamic model. The contact angle predicted by free energy minimization of the RD model neglecting the line tension (eq 4) is indistinguishable, within its error bar, from the angle measured in the simulations. The simulation results validate the use of Young equation to predict the morphology of two-phase large liquid droplets, with

Table 4. Contact Angles at 295 K Computed from Simulations with Various Water–Nonane Interaction Strengths ε_{wm} and Predicted from Surface Tensions by Young Equation

ε_{wm} (kcal/mol)	γ_{wn} (mJ/m^2)	θ from eq 4 (deg)	θ from simulations (deg)
0.15	60 ± 1.2	75 ± 6	75 ± 1
0.17	51 ± 1.2	49 ± 9	53 ± 1
0.18	48 ± 1.2	38 ± 12	41 ± 1
0.20	40 ± 1.2	0 (core–shell)	0 (core–shell)

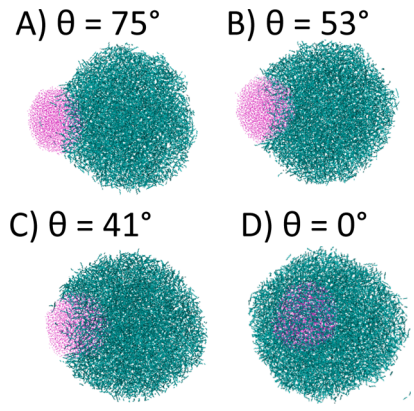

Figure 6. Snapshots of water–nonane droplets with tuned ε_{wm} interactions strength (Table 4) to produce a set of water–nonane surface tensions γ_{wn}: (A) 60 mJ/m^2, (B) 51 mJ/m^2, (C) 48 mJ/m^2, (D) 40 mJ/m^2. All droplets are at 295 K and contain 4000 water (pink points) and 4000 nonane (cyan lines) molecules. The contact angles measured in the molecular simulations (shown by the labels of each snapshot) are in excellent agreement with those predicted by eq 4 (see Table 4).

DOI: 10.1021/jacs.5b05579
J. Am. Chem. Soc. 2015, 137, 10642–10651

the line tension generally acting as a small correction term that is significant only for small nanodroplets.

4. CONCLUSIONS

The morphology of mixed-phase atmospheric aerosols can have a significant effect on their rate of water and gas uptake and the type and rate of heterogeneous reactions they promote. It is difficult, however, to predict whether aerosols of a given global composition will undergo liquid−liquid phase separation.[21,23,34−61] Moreover, when phase-separation occurs it is very challenging to accurately determine the morphologies of the aerosols in experiments.[63] Atmospheric aerosols between 100 nm and 2.5 μm are the longest lived in the atmosphere.[129] In this work we demonstrate that the extent of wetting in complex liquid−liquid phase separated atmospheric aerosols larger than ∼100 nm diameter can be accurately predicted from knowledge of the liquid−vapor and liquid−liquid surface tensions of the pair of liquids. We derive the equilibrium morphology of aerosols that contain two liquid phases by minimization of the free energy of the idealized Russian doll (RD) or lens on a sphere model as a function of the contact angle between the two liquids. Molecular simulations of a wide range of liquid−liquid separated droplets verify that RD is a very good model for their internal structure. We demonstrate that Young relation provides the exact solution of the contact angle between the two phases in lens on a sphere droplets. We propose that optimization of the exact degree of curvature of the liquid−liquid interface can be attained by considering Neumann's triangle construction. The latter is the solution for the elastocapillary equilibrium when elastic forces are negligible and the morphology of the droplet is completely determined by capillary forces. Young equation, on the other hand, corresponds to the limit in which one of the phases has significant shear modulus and cannot be deformed. The contact angles predicted by Young (eq 4) and Neumann (eq 5) relations, however, are always very close (Table 1). The validity of these equations for liquid−liquid separated aerosols implies that the contact angle depends on the composition of the liquids but not on the amount of each phase in the droplet, and it provides an easy, analytical method, for predicting the morphology of complex aerosols.

To accurately predict the morphology of small nanodroplets, we account for the effect of the line tension τ on the free energy. Our results indicate that τ can alter the morphologies of common liquid nanodroplets between partial wetting and core−shell structure. Line tension effects can be pronounced in droplets of about 10 nm diameter, particularly for those close to the limits between core−shell and partial wetting or nonwetting and partial wetting, but become negligible already for ∼100 nm diameter aerosols. We validate the thermodynamic predictions with molecular simulations of water−nonane droplets, for which we compute a line tension in agreement with estimates from theory and analysis of experimental data.

We build morphology maps (Figures 2 and 3) in which we locate aerosols for which the surface tensions have been determined in experiments. Interestingly, we find that all liquid−liquid separated model atmospheric aerosols studied to date are located near the boundary between partial wetting and total wetting, with contact angles rarely larger than 30°. Even aerosols made of long chain alkanes and water are very close to the boundary between partial wetting and total wetting: alkanes are not hydrophobic enough to result in demixing into two one-phase droplets. We do not expect any liquid−liquid separated atmospheric aerosols close to the boundary of the nonwetting domain. Our findings should have broad application for elucidating the kinetics of water and gas uptake of aerosols, and for constructing a predictive model for liquid aerosols in the atmosphere.

AUTHOR INFORMATION

Corresponding Author

*valeria.molinero@utah.edu

Notes

The authors declare no competing financial interest.

ACKNOWLEDGMENTS

This work was supported by the National Science Foundation through the Centers of Chemical Innovation Program under award CHE-1305427. We thank the Center for High performance Computing at the University of Utah for technical support and allocation of computer time. We gratefully acknowledge discussions with Gerald Wilemski, Alexei Tivanski, Holly Morris, and Vicki Grassian.

REFERENCES

(1) Yu, H.; Kaufman, Y. J.; Chin, M.; Feingold, G.; Remer, L. A.; Anderson, T. L.; Balkanski, Y.; Bellouin, N.; Boucher, O.; Christopher, S.; DeCola, P.; Kahn, R.; Koch, D.; Loeb, N.; Reddy, M. S.; Schulz, M.; Takemura, T.; Zhou, M. *Atmos. Chem. Phys.* **2006**, *6*, 613.

(2) Haywood, J.; Boucher, O. *Rev. Geophys.* **2000**, *38*, 513.

(3) Quinn, P. K.; Bates, T. S.; Schulz, K. S.; Coffman, D. J.; Frossard, A. A.; Russell, L. M.; Keene, W. C.; Kieber, D. J. *Nat. Geosci.* **2014**, *7*, 228.

(4) Collins, D. B.; Ault, A. P.; Moffet, R. C.; Ruppel, M. J.; Cuadra-Rodriguez, L. A.; Guasco, T. L.; Corrigan, C. E.; Pedler, B. E.; Azam, F.; Aluwihare, L. I.; Bertram, T. H.; Roberts, G. C.; Grassian, V. H.; Prather, K. A. *J. Geophys. Res.* **2013**, *118*, 8553.

(5) Moore, M. J. K.; Furutani, H.; Roberts, G. C.; Moffet, R. C.; Gilles, M. K.; Palenik, B.; Prather, K. A. *Atmos. Environ.* **2011**, *45*, 7462.

(6) Fuentes, E.; Coe, H.; Green, D.; McFiggans, G. *Atmos. Chem. Phys.* **2011**, *11*, 2585.

(7) Petters, M. D.; Kreidenweis, S. M. *Atmos. Chem. Phys.* **2007**, *7*, 1961.

(8) Pradeep Kumar, P.; Broekhuizen, K.; Abbatt, J. P. D. *Atmos. Chem. Phys.* **2003**, *3*, 509.

(9) Bilde, M.; Svenningsson, B. *Tellus, Ser. B* **2004**, *56*, 128.

(10) Sun, J.; Ariya, P. A. *Atmos. Environ.* **2006**, *40*, 795.

(11) Schnell, R. C.; Vali, G. *J. Atmos. Sci.* **1976**, *33*, 1554.

(12) Rosinski, J.; Haagenson, P. L.; Nagamoto, C. T.; Parungo, F. *J. Aerosol Sci.* **1987**, *18*, 291.

(13) Bigg, E. K. *J. Atmos. Sci.* **1973**, *30*, 1153.

(14) Baustian, K. J.; Wise, M. E.; Jensen, E. J.; Schill, G. P.; Freedman, M. A.; Tolbert, M. A. *Atmos. Chem. Phys.* **2013**, *13*, 5615.

(15) Schnell, R. C. *J. Atmos. Sci.* **1977**, *34*, 1299.

(16) Ault, A. P.; Guasco, T. L.; Baltrusaitis, J.; Ryder, O. S.; Trueblood, J. V.; Collins, D. B.; Ruppel, M. J.; Cuadra-Rodriguez, L. A.; Prather, K. A.; Grassian, V. H. *J. Phys. Chem. Lett.* **2014**, *5*, 2493.

(17) Prather, K. A.; Bertram, T. H.; Grassian, V. H.; Deane, G. B.; Stokes, M. D.; DeMott, P. J.; Aluwihare, L. I.; Palenik, B. P.; Azam, F.; Seinfeld, J. H.; Moffet, R. C.; Molina, M. J.; Cappa, C. D.; Geiger, F. M.; Roberts, G. C.; Russell, L. M.; Ault, A. P.; Baltrusaitis, J.; Collins, D. B.; Corrigan, C. E.; Cuadra-Rodriguez, L. A.; Ebben, C. J.; Forestieri, S. D.; Guasco, T. L.; Hersey, S. P.; Kim, M. J.; Lambert, W. F.; Modini, R. L.; Mui, W.; Pedler, B. E.; Ruppel, M. J.; Ryder, O. S.; Schoepp, N. G.; Sullivan, R. C.; Zhao, D. *Proc. Natl. Acad. Sci. U. S. A.* **2013**, *110*, 7550.

(18) Laskin, J.; Laskin, A.; Nizkorodov, S. A. *Int. Rev. Phys. Chem.* **2013**, *32*, 128.

DOI: 10.1021/jacs.5b05579
J. Am. Chem. Soc. 2015, 137, 10642−10651

(19) Finlayson-Pitts, B. J. *Phys. Chem. Chem. Phys.* **2009**, *11*, 7760.
(20) Ryder, O. S.; Ault, A. P.; Cahill, J. F.; Guasco, T. L.; Riedel, T. P.; Cuadra-Rodriguez, L. A.; Gaston, C. J.; Fitzgerald, E.; Lee, C.; Prather, K. A.; Bertram, T. H. *Environ. Sci. Technol.* **2014**, *48*, 1618.
(21) Zuend, A.; Seinfeld, J. H. *Atmos. Chem. Phys.* **2012**, *12*, 3857.
(22) Fuzzi, S.; Andreae, M. O.; Huebert, B. J.; Kulmala, M.; Bond, T. C.; Boy, M.; Doherty, S. J.; Guenther, A.; Kanakidou, M.; Kawamura, K.; Kerminen, V. M.; Lohmann, U.; Russell, L. M.; Pöschl, U. *Atmos. Chem. Phys.* **2006**, *6*, 2017.
(23) You, Y.; Renbaum-Wolff, L.; Carreras-Sospedra, M.; Hanna, S. J.; Hiranuma, N.; Kamal, S.; Smith, M. L.; Zhang, X.; Weber, R. J.; Shilling, J. E.; Dabdub, D.; Martin, S. T.; Bertram, A. K. *Proc. Natl. Acad. Sci. U. S. A.* **2012**, *109*, 13188.
(24) Folkers, M. *Geophys. Res. Lett.* **2003**, *30*, 1644.
(25) Anttila, T.; Kiendler-Scharr, A.; Tillmann, R.; Mentel, T. F. *J. Phys. Chem. A* **2006**, *110*, 10435.
(26) Park, S.-C.; Burden, D. K.; Nathanson, G. M. *J. Phys. Chem. A* **2007**, *111*, 2921.
(27) Cosman, L. M.; Bertram, A. K. *J. Phys. Chem. A* **2008**, *112*, 4625.
(28) Escorcia, E. N.; Sjostedt, S. J.; Abbatt, J. P. D. *J. Phys. Chem. A* **2010**, *114*, 13113.
(29) Gaston, C. J.; Thornton, J. A.; Ng, N. L. *Atmos. Chem. Phys.* **2014**, *14*, 5693.
(30) McNeill, V. F.; Patterson, J.; Wolfe, G. M.; Thornton, J. A. *Atmos. Chem. Phys.* **2006**, *6*, 1635.
(31) Thornton, J. A.; Abbatt, J. P. D. *J. Phys. Chem. A* **2005**, *109*, 10004.
(32) Ault, A. P.; Zhao, D.; Ebben, C. J.; Tauber, M. J.; Geiger, F. M.; Prather, K. A.; Grassian, V. H. *Phys. Chem. Chem. Phys.* **2013**, *15*, 6206.
(33) De Leeuw, G.; Andreas, E. L.; Anguelova, M. D.; Fairall, C. W.; Lewis, E. R.; O'Dowd, C.; Schulz, M.; Schwartz, S. E. *Rev. Geophys.* **2011**, DOI: 10.1029/2010RG000349.
(34) Marcolli, C.; Krieger, U. K. *J. Phys. Chem. A* **2006**, *110*, 1881.
(35) Anttila, T.; Kiendler-Scharr, A.; Mentel, T. F.; Tillmann, R. *J. Atmos. Chem.* **2007**, *57*, 215.
(36) Buajarern, J.; Mitchem, L.; Reid, J. P. *J. Phys. Chem. A* **2007**, *111*, 9054.
(37) Ciobanu, V. G.; Marcolli, C.; Krieger, U. K.; Weers, U.; Peter, T. *J. Phys. Chem. A* **2009**, *113*, 10966.
(38) Kwamena, N.-O. A.; Buajarern, J.; Reid, J. P. *J. Phys. Chem. A* **2010**, *114*, 5787.
(39) Zuend, A.; Marcolli, C.; Peter, T.; Seinfeld, J. H. *Atmos. Chem. Phys.* **2010**, *10*, 7795.
(40) Zuend, A.; Marcolli, C.; Booth, A. M.; Lienhard, D. M.; Soonsin, V.; Krieger, U. K.; Topping, D. O.; McFiggans, G.; Peter, T.; Seinfeld, J. H. *Atmos. Chem. Phys.* **2011**, *11*, 9155.
(41) Bertram, A. K.; Martin, S. T.; Hanna, S. J.; Smith, M. L.; Bodsworth, A.; Chen, Q.; Kuwata, M.; Liu, A.; You, Y.; Zorn, S. R. *Atmos. Chem. Phys.* **2011**, *11*, 10995.
(42) Reid, J. P.; Dennis-Smither, B. J.; Kwamena, N.-O. A.; Miles, R. E. H.; Hanford, K. L.; Homer, C. J. *Phys. Chem. Chem. Phys.* **2011**, *13*, 15559.
(43) Smith, M. L.; Kuwata, M.; Martin, S. T. *Aerosol Sci. Technol.* **2011**, *45*, 244.
(44) Krieger, U. K.; Marcolli, C.; Reid, J. P. *Chem. Soc. Rev.* **2012**, *41*, 6631.
(45) Pöhlker, C.; Wiedemann, K. T.; Sinha, B.; Shiraiwa, M.; Gunthe, S. S.; Smith, M.; Su, H.; Artaxo, P.; Chen, Q.; Cheng, Y.; Elbert, W.; Gilles, M. K.; Kilcoyne, A. L. D.; Moffet, R. C.; Weigand, M.; Martin, S. T.; Pöschl, U.; Andreae, M. O. *Science* **2012**, *337*, 1075.
(46) Song, M.; Marcolli, C.; Krieger, U. K.; Lienhard, D. M.; Peter, T. *Faraday Discuss.* **2013**, *165*, 289.
(47) Shiraiwa, M.; Zuend, A.; Bertram, A. K.; Seinfeld, J. H. *Phys. Chem. Chem. Phys.* **2013**, *15*, 11441.
(48) Veghte, D. P.; Altaf, M. B.; Freedman, M. A. *J. Am. Chem. Soc.* **2013**, *135*, 16046.
(49) Zuend, A.; Seinfeld, J. H. *Fluid Phase Equilib.* **2013**, *337*, 201.
(50) Veghte, D. P.; Bittner, D. R.; Freedman, M. A. *Anal. Chem.* **2014**, *86*, 2436.
(51) You, Y.; Bertram, A. K. *Atmos. Chem. Phys.* **2015**, *15*, 1351.
(52) Zuend, A.; Marcolli, C.; Luo, B. P.; Peter, T. *Atmos. Chem. Phys.* **2008**, *8*, 4559.
(53) You, Y.; Renbaum-Wolff, L.; Bertram, A. K. *Atmos. Chem. Phys.* **2013**, *13*, 11723.
(54) Drozd, G. T.; Woo, J. L.; McNeill, V. F. *Atmos. Chem. Phys.* **2013**, *13*, 8255.
(55) Song, M.; Marcolli, C.; Krieger, U. K.; Zuend, A.; Peter, T. *Atmos. Chem. Phys.* **2012**, *12*, 2691.
(56) Song, M.; Marcolli, C.; Krieger, U. K.; Zuend, A.; Peter, T. *Geophys. Res. Lett.* **2012**, DOI: 10.1029/2012GL052807.
(57) Smith, M. L.; Bertram, A. K.; Martin, S. T. *Atmos. Chem. Phys.* **2012**, *12*, 9613.
(58) Prisle, N. L.; Engelhart, G. J.; Bilde, M.; Donahue, N. M. *Geophys. Res. Lett.* **2010**, *37*, L01802.
(59) Clegg, S. L.; Seinfeld, J. H.; Brimblecombe, P. *J. Aerosol Sci.* **2001**, *32*, 713.
(60) Pankow, J. F. *Atmos. Environ.* **2003**, *37*, 3323.
(61) O'Brien, R. E.; Wang, B.; Kelly, S. T.; Lundt, N.; You, Y.; Bertram, A. K.; Leone, S. R.; Laskin, A.; Gilles, M. K. *Environ. Sci. Technol.* **2015**, *49*, 4995.
(62) Ma, X.; Chakraborty, P.; Henz, B. J.; Zachariah, M. R. *Phys. Chem. Chem. Phys.* **2011**, *13*, 9374.
(63) You, Y.; Smith, M. L.; Song, M.; Martin, S. T.; Bertram, A. K. *Int. Rev. Phys. Chem.* **2014**, *33*, 43.
(64) Lee, L. L. *Fluid Phase Equilib.* **1997**, *131*, 67.
(65) Long, F. A.; McDevit, W. F. *Chem. Rev.* **1952**, *51*, 119.
(66) Grover, P. K.; Ryall, R. L. *Chem. Rev.* **2005**, *105*, 1.
(67) Pathak, H.; Obeidat, A.; Wilemski, G.; Wyslouzil, B. *J. Chem. Phys.* **2014**, *140*, 224318.
(68) Zhou, Q.; Pang, S.-F.; Wang, Y.; Ma, J.-B.; Zhang, Y.-H. *J. Phys. Chem. B* **2014**, *118*, 6198.
(69) Pathak, H.; Wyslouzil, B.; Obeidat, A.; Wilemski, G. *AIP Conf. Proc.* **2013**, *1527*, 472.
(70) Obeidat, A.; Hrahsheh, F.; Wilemski, G. *J. Phys. Chem. B* **2015**, *119*, 9304−9311.
(71) Torza, S.; Mason, S. G. *J. Colloid Interface Sci.* **1970**, *33*, 67.
(72) Factorovich, M. H.; Molinero, V.; Scherlis, D. A. *J. Am. Chem. Soc.* **2014**, *136*, 4508.
(73) Dussaud, A.; Vignes-Adler, M. *Langmuir* **1997**, *13*, 581.
(74) Dobbs, H. *Langmuir* **1999**, *15*, 2586.
(75) Wang, J. Y.; Betelu, S.; Law, B. M. *Phys. Rev. E: Stat. Phys., Plasmas, Fluids, Relat. Interdiscip. Top.* **2001**, *63*, 031601.
(76) Aveyard, R.; Clint, J. H.; Nees, D.; Paunov, V. *Colloids Surf., A* **1999**, *146*, 95.
(77) Wilemski, G. *Homogeneous Binary Nucleation Theory and the Structure of Binary Nanodroplets*; Springer: Dordrecht, the Netherlands, 2007.
(78) Cao, Z.; Dobrynin, A. V. *Macromolecules* **2015**, *48*, 443.
(79) Young, T. *Philos. Trans. R. Soc. London* **1805**, *95*, 65.
(80) Fletcher, N. H. *J. Chem. Phys.* **1958**, *29*, 572.
(81) Iwamatsu, M. *Langmuir* **2015**, *31*, 3861.
(82) Hienola, A. I.; Winkler, P. M.; Wagner, P. E.; Vehkamäki, H.; Lauri, A.; Napari, I.; Kulmala, M. *J. Chem. Phys.* **2007**, *126*, 094705.
(83) Qian, M.; Ma, J. *J. Chem. Phys.* **2009**, *130*, 214709.
(84) Rowlinson, J. S.; Widom, B. *Molecular Theory of Capillarity*; Oxford Univeristy Press: Oxford, 1989.
(85) Neumann, F. *Vorlesungen über die Theorie der Capillaritt*; Teubner, B.G.: Leipzig, 1894.
(86) Noirez, L.; Baroni, P. *J. Phys.: Condens. Matter* **2012**, *24*, 372101.
(87) Goebel, A.; Lunkenheimer, K. *Langmuir* **1997**, *13*, 369.
(88) Vargaftik, N. B.; Volkov, B. N.; Voljak, L. D. *J. Phys. Chem. Ref. Data* **1983**, *12*, 817.
(89) Arthur, W. Adamson, A. P. G. *Physical Chemistry of Surfaces*, 6th ed.; Wiley-Interscience: Hoboken, NJ, 1997.
(90) Morris, H. S.; Grassian, V. H.; Tivanski, A. V. *Chem. Sci.* **2015**, *6*, 3242.
(91) Tervahattu, H. *J. Geophys. Res.* **2002**, *107*, 4319.

DOI: 10.1021/jacs.5b05579
J. Am. Chem. Soc. 2015, 137, 10642−10651

(92) Tervahattu, H.; Juhanoja, J.; Vaida, V.; Tuck, A. F.; Niemi, J. V.; Kupiainen, K.; Kulmala, M.; Vehkamäki, H. *J. Geophys. Res.* **2005**, *110*, 1.
(93) Donaldson, D. J.; George, C. *Environ. Sci. Technol.* **2012**, *46*, 10385.
(94) Dilbeck, C. W.; Finlayson-Pitts, B. J. *Phys. Chem. Chem. Phys.* **2013**, *15*, 9833.
(95) Mochida, M.; Kitamori, Y.; Kawamura, K.; Nojiri, Y.; Suzuki, K. *J. Geophys. Res.* **2002**, *107*, 4325.
(96) Pathak, H.; Wölk, J.; Strey, R.; Wyslouzil, B. E. *J. Chem. Phys.* **2014**, *140*, 034304.
(97) Zeppieri, S.; Rodríguez, J.; López de Ramos, A. L. *J. Chem. Eng. Data* **2001**, *46*, 1086.
(98) Jasper, J. J.; Kring, E. V. *J. Phys. Chem.* **1955**, *59*, 1019.
(99) Plimpton, S. *J. Comput. Phys.* **1995**, *117*, 1.
(100) Jorgensen, W. L.; Madura, J. D.; Swenson, C. J. *J. Am. Chem. Soc.* **1984**, *106*, 6638.
(101) Jorgensen, W. L.; Tirado-Rives, J. *J. Am. Chem. Soc.* **1988**, *110*, 1657.
(102) Molinero, V.; Moore, E. B. *J. Phys. Chem. B* **2009**, *113*, 4008.
(103) de la Llave, E.; Molinero, V.; Scherlis, D. A. *J. Chem. Phys.* **2010**, *133*, 034513.
(104) Jacobson, L. C.; Molinero, V. *J. Phys. Chem. B* **2010**, *114*, 7302.
(105) Moore, E. B.; de la Llave, E.; Welke, K.; Scherlis, D. A.; Molinero, V. *Phys. Chem. Chem. Phys.* **2010**, *12*, 4124.
(106) Moore, E. B.; Molinero, V. *J. Chem. Phys.* **2010**, *132*, 244504.
(107) González Solveyra, E. a.; de la Llave, E.; Scherlis, D. A.; Molinero, V. *J. Phys. Chem. B* **2011**, *115*, 14196.
(108) Moore, E. B.; Molinero, V. *Phys. Chem. Chem. Phys.* **2011**, *13*, 20008.
(109) Moore, E. B.; Molinero, V. *Nature* **2011**, *479*, 506.
(110) Baron, R.; Molinero, V. *J. Chem. Theory Comput.* **2012**, *8*, 3696.
(111) De La Llave, E.; Molinero, V.; Scherlis, D. A. *J. Phys. Chem. C* **2012**, *116*, 1833.
(112) Johnston, J. C.; Molinero, V. *J. Am. Chem. Soc.* **2012**, *134*, 6650.
(113) Shepherd, T. D.; Koc, M. A.; Molinero, V. *J. Phys. Chem. C* **2012**, *116*, 12172.
(114) Moore, E. B.; Allen, J. T.; Molinero, V. *J. Phys. Chem. C* **2012**, *116*, 7507.
(115) Solveyra, E. G.; Llave, E. d. l.; Molinero, V.; Soler-Illia, G. J. A. A.; Scherlis, D. A. *J. Phys. Chem. C* **2013**, *117*, 3330.
(116) Song, B.; Molinero, V. *J. Chem. Phys.* **2013**, *139*, 054511.
(117) Factorovich, M. H.; Molinero, V.; Scherlis, D. A. *J. Chem. Phys.* **2014**, *140*, 064111.
(118) Jacobson, L. C.; Kirby, R. M.; Molinero, V. *J. Phys. Chem. B* **2014**, *118*, 8190.
(119) Lu, J.; Qiu, Y.; Baron, R.; Molinero, V. *J. Chem. Theory Comput.* **2014**, *10*, 4104.
(120) Lupi, L.; Hudait, A.; Molinero, V. *J. Am. Chem. Soc.* **2014**, *136*, 3156.
(121) Lupi, L.; Kastelowitz, N.; Molinero, V. *J. Chem. Phys.* **2014**, *141*, 18C508.
(122) Lupi, L.; Molinero, V. *J. Phys. Chem. A* **2014**, *118*, 7330.
(123) Moore, E. B.; Molinero, V. *J. Chem. Phys.* **2009**, *130*, 244505.
(124) Hudait, A.; Molinero, V. *J. Am. Chem. Soc.* **2014**, *136*, 8081.
(125) Gloor, G. J.; Jackson, G.; Blas, F. J.; de Miguel, E. *J. Chem. Phys.* **2005**, *123*, 134703.
(126) Berendsen, H. J. C.; Grigera, J. R.; Straatsma, T. P. *J. Phys. Chem.* **1987**, *91*, 6269.
(127) Hrahsheh, F.; Wilemski, G. *AIP Conf. Proc.* **2013**, *1527*, 63.
(128) Chen, P.; Gaydos, J.; Neumann, A. W. *Langmuir* **1996**, *12*, 5956.
(129) Seinfeld, J. H.; Pandis, S. N. *Atomospheric Chemistry and Physics: From Air Pollution to Climate Change*, 2nd ed.; Wiley: Hoboken, NJ, 2006.

DOI: 10.1021/jacs.5b05579
J. Am. Chem. Soc. 2015, 137, 10642−10651